LETTER

Responsive biomimetic networks from polyisocyanopeptide hydrogels

Paul H. J. Kouwer[1]*, Matthieu Koepf[1]*, Vincent A. A. Le Sage[1], Maarten Jaspers[1], Arend M. van Buul[1], Zaskia H. Eksteen-Akeroyd[1], Tim Woltinge[1], Erik Schwartz[1], Heather J. Kitto[1], Richard Hoogenboom[1]†, Stephen J. Picken[2], Roeland J. M. Nolte[1], Eduardo Mendes[2] & Alan E. Rowan[1]

Mechanical responsiveness is essential to all biological systems down to the level of tissues and cells[1,2]. The intra- and extracellular mechanics of such systems are governed by a series of proteins, such as microtubules, actin, intermediate filaments and collagen[3,4]. As a general design motif, these proteins self-assemble into helical structures and superstructures that differ in diameter and persistence length to cover the full mechanical spectrum[1]. Gels of cytoskeletal proteins display particular mechanical responses (stress stiffening) that until now have been absent in synthetic polymeric and low-molar-mass gels. Here we present synthetic gels that mimic in nearly all aspects gels prepared from intermediate filaments. They are prepared from polyisocyanopeptides[5–7] grafted with oligo(ethylene glycol) side chains. These responsive polymers possess a stiff and helical architecture, and show a tunable thermal transition where the chains bundle together to generate transparent gels at extremely low concentrations. Using characterization techniques operating at different length scales (for example, macroscopic rheology, atomic force microscopy and molecular force spectroscopy) combined with an appropriate theoretical network model[8–10], we establish the hierarchical relationship between the bulk mechanical properties and the single-molecule parameters. Our results show that to develop artificial cytoskeletal or extracellular matrix mimics, the essential design parameters are not only the molecular stiffness, but also the extent of bundling. In contrast to the peptidic materials, our polyisocyanide polymers are readily modified, giving a starting point for functional biomimetic hydrogels with potentially a wide variety of applications[11–14], in particular in the biomedical field.

The artificial gels are based on polyisocyanopeptides (PICs), composed of a β-helical architecture stabilized by a peptidic hydrogen-bond network along the polymer backbone[6]. Polymers **P1–P3** were obtained through a nickel(II)-catalysed polymerization of di-, tri- and tetraethylene glycol functionalized isocyano-(D)-alanyl-(L)-alanines **1–3** (Fig. 1)[15]. Variation of the catalyst to monomer ratio allowed us to tune the molecular weights of the polymers (see Supplementary Information). The hydrogen-bonded helical structure of the polymer
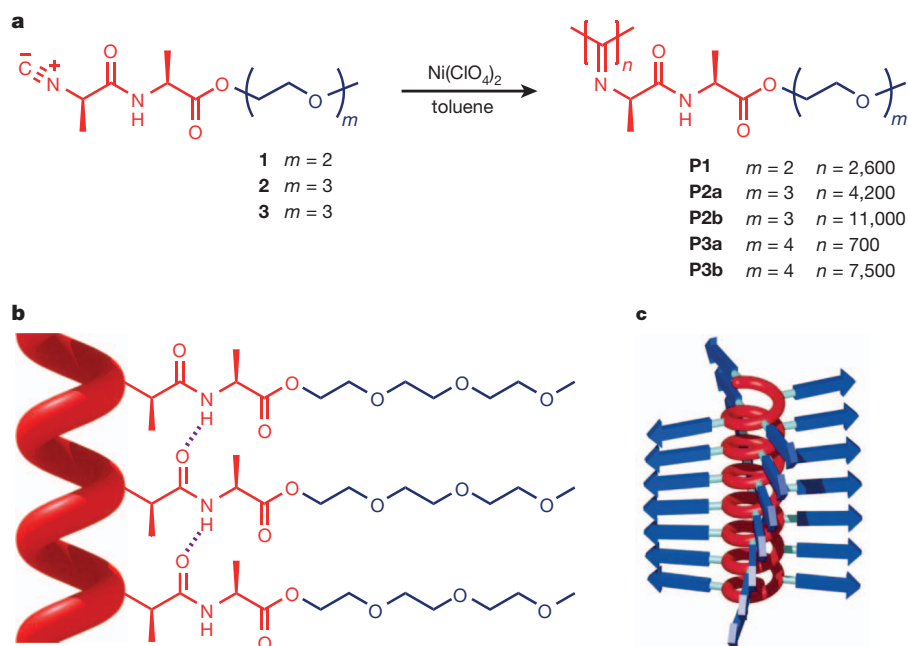
1	$m = 2$	
2	$m = 3$	
3	$m = 3$	

P1	$m = 2$	$n = 2,600$
P2a	$m = 3$	$n = 4,200$
P2b	$m = 3$	$n = 11,000$
P3a	$m = 4$	$n = 700$
P3b	$m = 4$	$n = 7,500$

Figure 1 | Oligo(ethylene glycol)-substituted PICs. a, Synthesis of the polymers—the degree of polymerization is estimated from atomic force microscopy (AFM) experiments. **b**, Representation of the hydrogen-bond network (dotted lines) that stabilizes the secondary helical structure for **P2**. **c**, Schematic illustration of the 4_1 β-sheet helix. Colour coding: red, the stiff helical polyisocyanide backbone stabilized with the hydrogen-bonded dialanyl groups; in **b** and **c** the backbone is schematically shown as a helix. Blue, the ethylene glycol peptide substituent 'tails', represented in **c** by blue arrows. Panel **c** is from ref. 6, reprinted with permission from AAAS.

[1]Radboud University Nijmegen, Institute for Molecules and Materials, Department of Molecular Materials, Heyendaalseweg 135, 6525 AJ Nijmegen, The Netherlands. [2]Delft University of Technology, Department of NanoStructured Materials, Julianalaan 136, 2628 BL Delft, The Netherlands. †Present address: Supramolecular Chemistry Group, Department of Organic Chemistry, Ghent University, Krijgslaan 281-S4, 9000 Ghent, Belgium.
*These authors contributed equally to this work.

backbone was confirmed by infrared and circular dichroism (Supplementary Fig. 1) spectroscopies. In aqueous solution and in the gel phase, the secondary structure of the polymer is stable up to about 70 °C as shown with circular dichroism experiments (Supplementary Figs 2 and 3). The combination of a densely packed helical structure and the strong intramolecular hydrogen bonds gives stiff polymer chains that are readily visualized by atomic force microscopy (AFM; Fig. 2a and Supplementary Fig. 4).

Thermal analysis of dilute aqueous solutions of **P2b** and **P3b** showed the formation of transparent hydrogels on heating at 18 and 44 °C, respectively. Polymers **P2a** and **P3a** did not form gels, but precipitated at these temperatures forming a cloudy suspension, whereas **P1** failed to dissolve in water (we attribute this to a transition temperature below 0 °C). The sol–gel phase transition was very fast (on a timescale of seconds) and fully reversible (Supplementary Fig. 13). The structure of the gel was visualized by AFM (Fig. 2b and Supplementary Fig. 5a–f) and cryo scanning electron microscopy (SEM; Supplementary Fig. 5g). Both techniques showed a network composed of bundles of polymer chains. The extent of bundling was estimated by statistical analysis of the AFM images of the bundles and the isolated polymer chains (Fig. 2c). The narrow distributions of relative heights was used to abstract the bundle number (average number of polymer chains per bundle) $N = 6.9$, using the relation $N = d_B^2/d_0^2 \approx h_B^2/h_0^2$, in which d_0 and d_B are the diameters, and h_0 and h_B the heights, of isolated chains and bundles, respectively.

We found that the bundle dimensions were constant irrespective of the polymer concentration. AFM analysis (Supplementary Fig. 6) of samples at higher concentration shows more rather than thicker bundles, which is also indicated by preliminary single-particle tracking studies of gels of **P2b** that show nanoparticle diffusion coefficients that strongly scale with concentration (Supplementary Fig. 7). The latter confirms that at higher concentrations more bundles (and hence smaller pores, which result in restricted particle displacement) are formed. This self-limiting behaviour of bundle formation is thought to be related to the chiral nature (that is, the helicity) and the intrinsic stiffness of the polymer molecules[16]. As a consequence of the fixed bundle size, the average pore size in the gel is directly controlled by the polymer concentration. Chain bundling is commonly observed for cytoskeletal polymers and the bundle properties (dimensions,
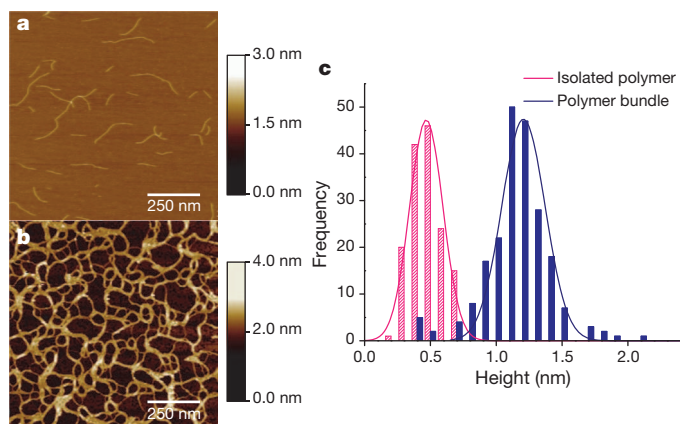
stiffness) are critical parameters in the mechanical properties of those gels. For gels based on actin or intermediate filaments, bundling is controlled by additives, ranging from binding proteins[17] to divalent metal ions[18], whereas bundle formation in the PIC gels is thermally activated.

The process of thermally induced gel formation is attributed to hydrophobic effects caused by the ethylene glycol tails grafted onto the polyisocyanide backbone. Flexible oligo(ethylene glycol) grafted polymers have been reported to show sharp order–disorder phase transitions at the lower critical solution temperature (LCST)[19]. Previous studies have demonstrated a linear relationship between the transition temperature and the average length of the ethylene glycol tail over a broad temperature range[20]. Heating **P2** and **P3** results in the entropic desolvation of the ethylene glycol arms, giving rise to more hydrophobic chains that separate from the aqueous solution. Indeed, the low molar mass polymers **P2a** and **P3a** precipitate at the LCST, whereas longer polymers yield completely transparent gels at the transition, as the long chains are kinetically trapped in a network structure before they precipitate. Even at very low concentrations, the gels are able to support their own weight during vial inversion tests; a sample of **P2b** passed the test at concentrations as low as 0.006 wt%, (Supplementary Fig. 8), which is about an order of magnitude lower in concentration than many of the well-known synthetic superhydrogelators[21].

To learn more about their mechanical properties, the polymer gels were subjected to a full variable temperature rheological analysis. Samples were measured in a Couette configuration with small oscillatory deformations at different frequencies and amplitudes in the linear response regime (Supplementary Figs 9 and 10). A broad-range frequency sweep in the gel phase (Supplementary Fig. 10) corroborates that the crosslinks formed at the LCST are permanent in nature. Temperature sweeps of **P2b** and **P3b** (Fig. 3a and Supplementary Fig. 11) show, at low temperatures, liquid-like behaviour with a storage modulus G' lower than the loss modulus G''. The temperature of the sharp transition that marks gel formation depends on the length of the ethylene glycol tail. It shows little dependence on the polymer concentration c. At elevated temperatures G' levels off to a plateau G_0; its absolute value, however, scales strongly with c. Analysis showed a power-law behaviour, $G_0 \propto c^n$ with coefficients n of 2.2 and 2.7 for **P2b** and **P3b**, respectively. These experimental values are in line with the theory of permanently linked semi-flexible networks that display purely entropic elasticity[9] (in which $n = 11/5$), and with other experimental studies based on cross-linked cytoskeletal proteins like actin[10] and intermediate-filament gels[8] (with $n = 2-2.5$), and also with other stiff materials such as DNA gels ($n = 2.3$)[22].

Unlike many gels of synthetic polymers, biopolymer gels show a strong, and well-defined, nonlinear stress response after a critical stress σ_c has been applied[4] (stress-stiffening). Although its origins are currently being debated[4,23,24], the effect is well described experimentally[4,8,9]. In the nonlinear regime, a small increase in the strain γ gives very high stress levels and often results in the rupture of the gel. To probe this regime carefully, we used a recently benchmarked pre-stress protocol[25] and determined the differential modulus K (the real part of which is defined as $K' = d\sigma/d\gamma$) as a function of applied stress σ (Fig. 3b). When scaled to G_0 and σ_c (Fig. 3c) all curves of **P2b** at different concentrations and temperatures reduce to a single master curve, displaying the theoretically predicted $K' \propto \sigma^{3/2}$ dependency[8]. The PIC-based gels show a quantitative resemblance to the protein-based biogels, even in the nonlinear regime.

A theoretical model for semi-flexible networks, based on the extensible worm-like chain model[26], has been developed to explain the mechanical behaviour of actin[9] and intermediate-filament-based hydrogels[9]. This model considers the network as a collection of thermally fluctuating bundles, with l_c as the average length between the crosslinks between bundles. We have modified the existing network model[23] to quantitatively describe the unusual experimentally observed thermal behaviour and to account for the fact that the bundle size in our system
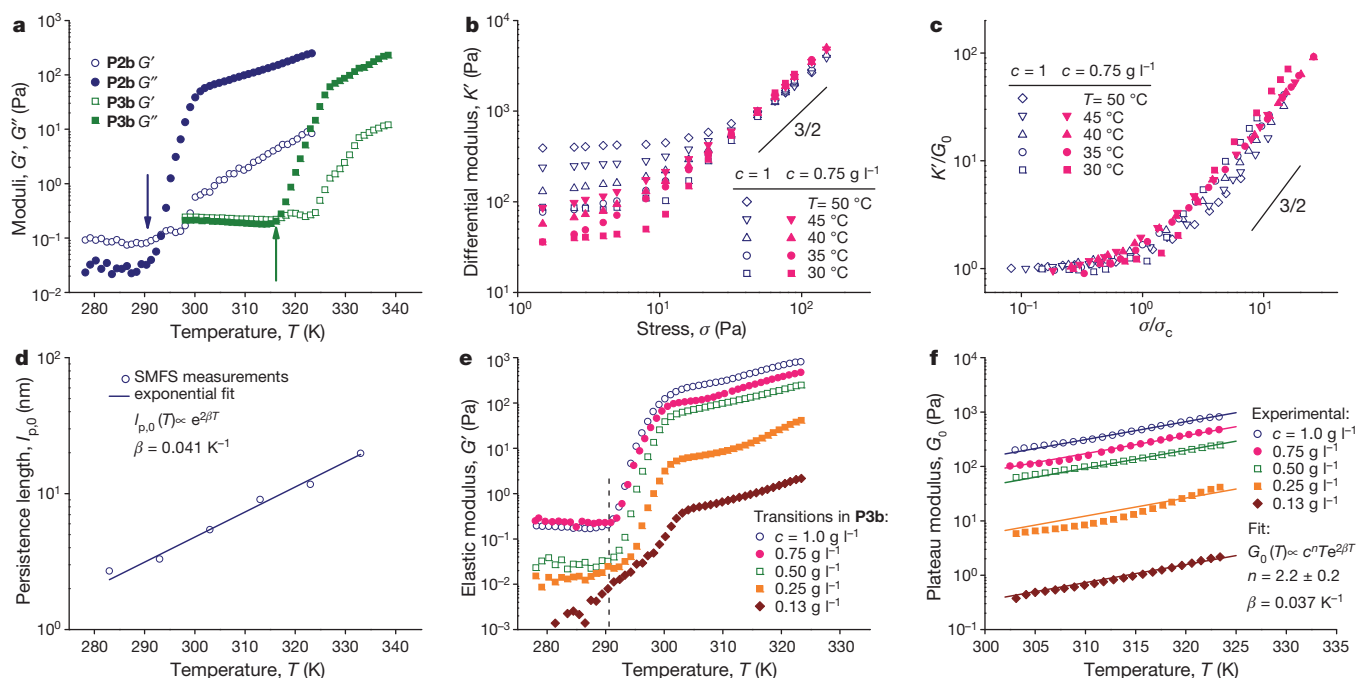

Figure 2 | AFM analysis of polymers and gel. a, AFM image of isolated polymer chains of **P2b**, spin-coated from an organic solution on mica. Colour scale here and in **b** shows height. **b**, AFM image of a 'monolayer' of bundles of the **P2b** gel transferred to mica. Occasional non-bundled polymers are visible. **c**, Statistical height histograms of both isolated chains (pink) and bundles (blue). Both show similarly narrow Gaussian distributions (see fits) with chain height $h_0 = 0.46 \pm 0.13$ nm and bundle height $h_B = 1.2 \pm 0.2$ nm. We note that the absolute height found by AFM is consistently too low. Considering that the diameter of the peptidic polymer without the ethylene glycol substituents is roughly 2 nm, only relative height distributions can be used to estimate the bundle numbers.

LETTER RESEARCH

Figure 3 | Rheological analysis of PIC gels. a, Moduli G' and G'' as a function of temperature T for **P2b** and **P3b** at $c = 1.0$ mg ml^{-1}. The arrows indicate the transition temperature, rheologically determined as the onset of the step in G' at $\omega = 6.2$ rad s^{-1} ($f = 1$ Hz, Supplementary Fig. 12). **b**, Differential modulus K' as a function of stress σ for different values of c and T. The model prediction $K' \propto \sigma^{3/2}$ is shown in **b** and **c**. **c**, Data scaled with the plateau modulus G_0 and the critical stress σ_c; all curves, independent of variations in c and T, collapse to a

single master curve. **d**, Single chain persistence length $l_{p,0}$ as a function of T of **P2b** between 10 and 60 °C measured by SMFS, fitted to a single exponential as shown. **e**, G' as a function of T for **P2b** at different concentrations. The dashed line at $T = 18$ °C shows that the onset of the gel temperature is nearly concentration-independent. **f**, G_0 as a function of T and exponential fits to n and β for different concentrations.

is independent of the concentration. The details of the model are given in the Supplementary Information. Not only does this model describe our experimental results accurately, it also yields information about the critical microscopic parameters—such as the persistence length of the bundles, $l_{p,B}$, and l_c. To extract this information, we apply equations (1) and (2) to the experimentally determined macroscopic quantities G_0 and σ_c:

$$G_0 = 6\chi \frac{c}{N} RT \frac{l_{p,B}^2}{l_c^3} \qquad (1)$$

$$\sigma_c = \chi \frac{c}{N} RT \frac{l_{p,B}}{l_c^2} \qquad (2)$$

Here, χ combines molecular constants, R is the gas constant and T is the absolute temperature. Equations (1) and (2) show that G_0 and σ_c depend on N, $l_{p,B}$ and l_c (l_c in turn also depends on concentration). Rheological measurements in the linear and nonlinear regimes, with c and T as experimental variables, in combination with variable temperature single molecule force spectroscopy (SMFS) measurements, allowed us to calculate $l_{p,B}$, l_c and N.

SMFM measurements[27] provide information on the persistence length of individual polymer chains, $l_{p,0}$. In these experiments we determined force–distance curves of dilute polymer samples and subjected the results to the same extensible worm-like chain model that was applied to analyse the rheological data. Subsequent statistical analysis of the experimental data provided the average values for $l_{p,0}$ (Supplementary Fig. 14). SMFS measurements on **P2b**, equilibrated in water, typically yielded modest values for $l_{p,0}$ (Fig. 3d)[27], which is attributed to water weakening the hydrogen-bond network along the polymer backbone (see Supplementary Information). A temperature sweep between 10 and 60 °C showed an exponential increase of the persistence length $l_{p,0}(T) \propto e^{\beta T}$ with an exponent β of 0.041 K^{-1}.

Figure 3e shows the plateau modulus $G_0(c,T)$ of **P2b** as obtained by bulk rheological temperature sweeps. At all c, G_0 showed an exponential increase with T (Fig. 3f); for this temperature range, the data were successfully fitted to $G_0(c,T) \propto c^n T e^{2\beta T}$ with exponents $n = 2.2$ and $2\beta = 0.073$ K^{-1}. In our system, the only temperature dependent contribution to G_0 is $l_{p,B}^2$ (equation (1)). The close match of the observed exponent from SFMS measurements and that from bulk rheology clearly indicates that the thermally induced increase in G_0 is simply the result of the stiffening of the individual polymer chains. This was confirmed by independent measurements of $\sigma_c(T)$ at different concentrations, which yielded a similar exponent, $\beta = 0.049$ K^{-1} (equation (2)).

Combining equations (1) and (2) returns $l_{p,B}$ as a function of N, G_0 and σ_c; the last two values were experimentally determined by bulk rheology in the linear and nonlinear regime. By taking $N \approx 7$, as obtained from AFM measurements, a value of $l_{p,B}$ of the order of hundreds of nanometres for **P2b** was found, about two orders of magnitude larger than $l_{p,0}$. This difference can only be rationalized by considering that the chains in the bundles are strongly interacting, and behave effectively as a single fibre with the constituent polymer chains 'glued' together. This so-called tight bundle regime is characterized by a square dependence of $l_{p,B}$ with N: $l_{p,B} = l_{p,0}N^2$; this is in contrast to the loose bundle regime, which shows a linear relationship[28]. Cross-linked biofibres, such as actin, show a transition from the tight to the loose bundle regime with increasing N. In line with these results, we also find a square dependence at low bundle numbers. By establishing the regime in which the bundles interact, we can now calculate N by the straightforward comparison of the SMFS results and the (nonlinear) rheology data. Under the standard conditions (1 mg ml^{-1}, 30 °C), we find $N = 9.1$, which agrees closely with the value estimated from the AFM measurements. Calculations of N at different temperatures and concentrations yield very consistent numbers, further highlighting that, for our materials, the bundle characteristics are

Table 1 | Comparison of hydrogels based on P2b and on neurofilaments

Characteristic gel property	P2b	Neurofilaments[3]
Bundle diameter, d_B	7.5 nm*	10 nm
Average bundle number, N	9	4
Persistence length†, $l_{p,B}$	460 nm	600 nm
Deformation regime ($G_0 \propto c^n$)	Entropic ($G_0 \propto c^{2.2}$)	Entropic ($G_0 \propto c^{2.5}$)
G_0†	100–1,000 Pa‡	2–20 Pa§
High-strain regime	Strain stiffening ($K' \propto \sigma^{3/2}$)	Strain stiffening ($K' \propto \sigma^{3/2}$)
Contour length†, l_c	110 nm	300 nm

Properties given in the first column were determined at similar concentrations; exceptions are shown by footnotes.
* Calculated based on N and an estimated cross-section of the polymers.
† Determined at 1 mg ml^{-1}.
‡ Temperature range: 30 °C < T < 60 °C.
§ Mg^{2+} concentration range: 2 mM < [Mg^{2+}] < 20 mM.

intrinsic polymer properties related to the secondary structure of the chains. After determination of N, equations (1) and (2) provide the other unknown quantities: $l_{p,B} = 460$ nm and $l_c = 110$ nm (at 1 mg ml^{-1}, 30 °C); the latter is significantly smaller than $l_{p,B}$, as would be expected for a semi-flexible network. The gels of **P2b** closely resemble those formed by neurofilaments (a typical class of intermediate filaments), not only in their mechanical properties, but also in their characteristic length scales—for example, bundle diameter, pore size and bundle stiffness (Table 1).

The model has now been modified to write G_0 and σ_c at given experimental conditions as a function of the intrinsic (temperature dependent) single-chain persistence length, the bundle number and the length between crosslinks (see Supplementary Information):

$$G_0(T) \propto N^3 \frac{c}{l_c^3} RT l_{p,0}^2(T) \qquad (3)$$

and

$$\sigma_c(T) \propto N \frac{c}{l_c^2} RT l_{p,0}(T) \qquad (4)$$
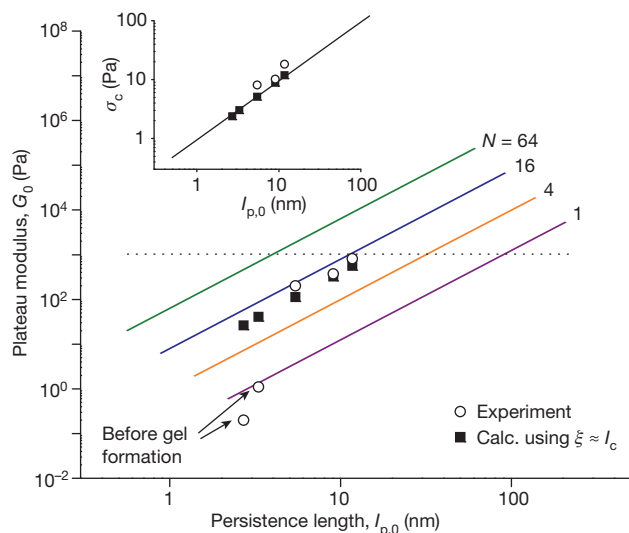

Figure 4 | Stiffness of the gel versus stiffness of the constituent polymer. Main panel: open circles show G_0 of **P2b** as a function of $l_{p,0}(T)$ at $T = 10$–60 °C and $c = 1$ mg ml^{-1}; filled squares show G_0 values of **P2b** calculated using equation (3) (substituting l_c for ξ) at the same temperatures and using $N = 9.1$. The coloured lines represent general trends, obtained from equation (3), which can be used to correlate $l_{p,0}$ to G_0 at a set concentration and given $N = 1$–64. The dotted line at $G_0 = 1$ kPa is shown for reference; it shows that 1-kPa gels can be prepared from a very stiff single polymer chain as well as from much more flexible, tightly bundled polymers (large N). The inset shows the variation of the calculated critical stress σ_c with $l_{p,0}$ (equation (4)), which is independent of N. The open circles are experimental data points obtained at $T = 30$, 40 and 50 °C. The corresponding calculated points (filled squares) overlap with the trend lines of $N = 1$–64.

Using equations (3) and (4) as a starting point, we can now speculate on how these hydrogels could be further engineered. For instance, is it possible to go even lower in concentration, can we set the pore size of a hydrogel, or can we generate stiffer gels that mimic the properties of the other cytoplasmic or extracellular materials?

To this end, we approximated the experimentally poorly accessible l_c (which scales with c as $l_c \propto c^{-0.4}$) by the mesh size ξ (which scales as $\xi \propto c^{-0.5}$, see Supplementary Information) that can be readily calculated from known molecular parameters, N and c ($\xi = 140$ nm for **P2b** at 1 mg ml^{-1}, 30 °C). When we further disregard the potential transition from the tight to the loose bundle regime, we can calculate G_0 as a function of the single chain persistence length $l_{p,0}$ and N (Fig. 4). The plot highlights that, even for intrinsically very stiff polymers, bundling is a prerequisite for good mechanical properties of the gel. Controlling bundling presents a central challenge for molecular chemists, because it allows tuning of both the gel modulus ($G_0 \propto \sqrt{N^3}$) and the pore size ($\xi \propto \sqrt{N}$) of the gel. This analysis is completely in line with how nature controls the mechanical properties of cytoskeletal soft materials: taking stiff protein elements (a variety of elements of different dimensions provide flexibility in the design) and controlling the amount of bundling by regulating the concentration of crosslinking proteins or divalent cations.

We have presented a truly artificial mimic of intermediate filaments, with all their characteristic mechanical properties. The helical poly-isocyanide polymer plays a crucial role in providing an intrinsically stiff backbone and controlling the bundling process. However, this class of materials goes beyond mimicking intermediate-filament bio-gels, because network characteristics can be readily manipulated through small modifications in the chemical structure—for instance, gel transition temperatures can be changed by the length of the ethylene glycol tail and the intrinsic backbone stiffness by the amino acid sequence[6,27]. Moreover, functional groups can be introduced at the periphery of the polymer which allows for the incorporation of a wide variety of (bio-)molecules or cross-linkers in the polymer, mimicking more closely the natural environment of the cell.

METHODS SUMMARY

Materials. The polymerization of **1**–**3** was carried out with Ni(ClO$_4$)$_2$·2H$_2$O as catalyst in toluene. The reaction mixtures were stirred vigorously in a sealed flask at room temperature for two hours. The solvent was removed and the residue was precipitated three times from chloroform or tetrahydrofuran in diethyl ether. The products were routinely characterized with infrared and circular dichroism spectroscopies, and AFM. NMR spectroscopy gives broad signals only.

AFM analysis. To visualize individual polymer chains, solutions (~1 µM in CHCl$_3$) were spin-coated on freshly cleaved muscovite mica substrates. Polymer gels were deposited on the substrate by direct contact transfer. All images were obtained by tapping mode AFM.

SMFS. Before analysis, the AFM tip was cleaned meticulously. Polymer samples (3 mM in CH$_2$Cl$_2$) were spin-coated on freshly cleaved muscovite mica. The substrate was rinsed with MilliQ water to remove non-absorbed polymer. After morphology and density characterization (tapping mode AFM in air), the SMFS measurements were conducted in MilliQ water. Owing to the low density on the surface, less than 1% of approach–retract cycles yielded successful traces.

Rheology. Samples were dissolved with regular vortexing in (cold) demineralized water at least 24 h before the measurements. Rheological measurements were

carried out in Couette geometry with heating/cooling rates of $2\,^{\circ}\mathrm{C}\,\mathrm{min}^{-1}$. Standard measurements were carried out at 4% strain and at different frequencies (0.5–5 Hz). The data shown in the manuscript was recorded at 1 Hz. For each sample, this was in the linear response regime. Nonlinear rheology in the gel phase was carried out at $50\,^{\circ}\mathrm{C}$ after equilibrating for 15 min using a pre-stress protocol[25]. A detailed description of all techniques and the modified semi-flexible network model is given in Supplementary Information.

1. Kamm, R. D. & Mofrad, M. R. K. in *Cytoskeletal Mechanics: Models and Measurements* (eds Mofrad, M. R. K. & Kamm, R. D.) Ch. 1, 1–17 (Cambridge Univ. Press, 2006).
2. Fernández, P., Pullarkat, P. A. & Ott, A. A master relation defines the nonlinear viscoelasticity of single fibroblasts. *Biophys. J.* **90,** 3796–3805 (2006).
3. Fernandez-Gonzalez, R. & Zallen, J. A. Feeling the squeeze: live-cell extrusion limits cell density in epithelia. *Cell* **149,** 965–967 (2012).
4. Storm, C., Pastore, J. J., MacKintosh, F. C., Lubensky, T. C. & Janmey, P. A. Nonlinear elasticity in biological gels. *Nature* **435,** 191–194 (2005).
5. Schwartz, E., Le Gac, S., Cornelissen, J. J. L. M., Nolte, R. J. M. & Rowan, A. E. Macromolecular multi-chromophoric scaffolding. *Chem. Soc. Rev.* **39,** 1576–1599 (2010).
6. Cornelissen, J. J. L. M. *et al.* β-helical polymers from isocyanopeptides. *Science* **293,** 676–680 (2001).
7. Keereweer, B. *et al.* in *Functional Supramolecular Architectures* Vol. 1 (eds Samori, P. & Cacialli, F.) Ch. 5, 135–152 (VCH, 2011).
8. Lin, Y.-C. *et al.* Origins of elasticity in intermediate filament networks. *Phys. Rev. Lett.* **104,** 058101 (2010).
9. MacKintosh, F. C., Kas, J. & Janmey, P. A. Elasticity of semiflexible biopolymer networks. *Phys. Rev. Lett.* **75,** 4425–4428 (1995).
10. Gardel, M. L. *et al.* Elastic behavior of cross-linked and bundled actin networks. *Science* **304,** 1301–1305 (2004).
11. Tiller, J. C. Increasing the local concentration of drugs by hydrogel formation. *Angew. Chem. Int. Edn* **42,** 3072–3075 (2003).
12. Place, E. S., Evans, N. D. & Stevens, M. M. Complexity in biomaterials for tissue engineering. *Nature Mater.* **8,** 457–470 (2009).
13. Peppas, N. A., Hilt, J. Z., Khademhosseini, A. & Langer, R. Hydrogels in biology and medicine: from molecular principles to bionanotechnology. *Adv. Mater.* **18,** 1345–1360 (2006).
14. Hirst, A. R., Escuder, B., Miravet, J. F. & Smith, D. K. High-tech applications of self-assembling supramolecular nanostructured gel-phase materials: from regenerative medicine to electronic devices. *Angew. Chem. Int. Edn* **47,** 8002–8018 (2008).
15. Rowan, A. E. *et al.* Method for the preparation of high molecular weight oligo(alkylene glycol) functionalized polyisocyanopeptides. European Patent 2,287,221 (2011).
16. Grason, G. M. & Bruinsma, R. F. Chirality and equilibrium biopolymer bundles. *Phys. Rev. Lett.* **99,** 098101 (2007).
17. Pollard, T. D. & Cooper, J. A. Actin and actin-binding proteins — a critical evaluation of mechanisms and functions. *Annu. Rev. Biochem.* **55,** 987–1035 (1986).
18. Leterrier, J. F., Kas, J., Hartwig, J., Vegners, R. & Janmey, P. A. Mechanical effects of neurofilament cross-bridges — modulation by phosphorylation, lipids, and interactions with F-actin. *J. Biochem.* **271,** 15687–15694 (1996).
19. Han, S., Hagiwara, M. & Ishizone, T. Synthesis of thermally sensitive water-soluble polymethacrylates by living anionic polymerizations of oligo(ethylene glycol) methyl ether methacrylates. *Macromolecules* **36,** 8312–8319 (2003).
20. Lutz, J. F. & Hoth, A. Preparation of ideal PEG analogues with a tunable thermosensitivity by controlled radical copolymerization of 2-(2-methoxyethoxy)ethyl methacrylate and oligo(ethylene glycol) methacrylate. *Macromolecules* **39,** 893–896 (2006).
21. Wang, H. *et al.* A structure-gelation ability study in a short peptide-based 'Super Hydrogelator' system. *Soft Matter* **7,** 3897–3905 (2011).
22. Mason, T. G., Dhople, A. & Wirtz, D. Linear viscoelastic moduli of concentrated DNA solutions. *Macromolecules* **31,** 3600–3603 (1998).
23. Onck, P. R., Koeman, T., van Dillen, T. & van der Giessen, E. Alternative explanation of stiffening in cross-linked semiflexible networks. *Phys. Rev. Lett.* **95,** 178102 (2005).
24. Huisman, E. M., van Dillen, T., Onck, P. R. & Van der Giessen, E. Three-dimensional cross-linked F-actin networks: relation between network architecture and mechanical behavior. *Phys. Rev. Lett.* **99,** 208103 (2007).
25. Broedersz, C. P. & MacKintosh, F. C. Molecular motors stiffen non-affine semiflexible polymer networks. *Soft Matter* **7,** 3186–3191 (2011).
26. Bustamante, C., Marko, J. F., Siggia, E. D. & Smith, S. Entropic elasticity of λ-phage DNA. *Science* **265,** 1599–1600 (1994).
27. Van Buul, A. M. *et al.* Stiffness versus architecture of single helical polyisocyanopeptides. *Chem. Sci.* (submitted).
28. Bathe, M., Heussinger, C., Claaessens, M. M. A. E., Bausch, A. R. & Frey, E. Cytoskeletal bundle mechanics. *Biophys. J.* **94,** 2955–2964 (2008).